

# Dynamic Magnetic Properties of $\text{La}_{0.8}\text{Ag}_{0.2}\text{MnO}_3$ Nanoparticles

Ali Rostamnejadi<sup>1</sup>

Received: 9 February 2016 / Accepted: 22 April 2016 / Published online: 29 April 2016  
© Springer Science+Business Media New York 2016

**Abstract** In this research, nanoparticles of  $\text{La}_{0.8}\text{Ag}_{0.2}\text{MnO}_3$  with mean particle sizes  $d$  of 16 and 22 nm have been prepared by sol-gel method. Dynamic magnetic properties of the samples have been carried out by AC magnetic susceptibility and electron spin resonance techniques. The structural properties of the samples have been characterized by X-ray diffraction using Rietveld refinement and transmission electron microscopy. The analysis of the AC magnetic susceptibility by phenomenological models reveals the interacting superparamagnetic behaviors in  $\text{La}_{0.8}\text{Ag}_{0.2}\text{MnO}_3$  nanoparticles. From the Vogel-Fulcher model, the values of  $1.3 \times 10^4$  and  $2.8 \times 10^4$  erg/cm<sup>3</sup> are obtained for the effective magnetic anisotropy constant for  $d = 16$  and 21 nm, respectively. Electron spin resonance signals of the samples are well described by double Lorentzian line shapes which suggest the presence of ferromagnetic clusters in the paramagnetic phase and possible phase separation at room temperature.

**Keywords** Manganite · Nanoparticles · Sol-gel · AC magnetic susceptibility · Superparamagnetism · Electron spin resonance · Phase separation

## 1 Introduction

Mixed valence manganites  $\text{La}_{1-x}\text{B}_x\text{MnO}_3$  ( $\text{B} = \text{Sr}, \text{Ba}, \text{Ca}, \text{Ag}, \text{K}$ ) have been widely studied due to their importance for fundamental research and possible potential applications [1–7]. The electrical and magnetic properties of manganites can be described by the double exchange model and taking into account the magnetic phase separation [1–3]. Magnetic nanoparticles of manganites exhibit unique phenomena such as large low-field magnetoresistance, low saturation magnetization, large magnetocaloric effect, exchange bias effect, superparamagnetic behavior, and superspin glass state [8–13]. Dynamic properties of magnetic nanoparticles are influenced by their intrinsic and extrinsic parameters. In general, the exchange interaction and the magnetic dipolar interparticle interaction play a significant role in the collective behavior of magnetic nanoparticle systems leading to superparamagnetic behavior or a superspin glass state [8, 9, 11, 14–23].

$\text{La}_{1-x}\text{Ag}_x\text{MnO}_3$  is a ferromagnetic material with colossal magnetoresistance and large magnetocaloric effects around room temperature [24–29]. While more studies have been focused on the bulk of  $\text{La}_{1-x}\text{Ag}_x\text{MnO}_3$ , less study has been carried out on its nanostructures. Due to the possible tuning of its Curie temperature, nanoparticles of  $\text{La}_{1-x}\text{Ag}_x\text{MnO}_3$  can be considered for low-field magnetoresistive sensors and biomedical applications [28, 30–32].

In this paper, dynamic magnetic properties of  $\text{La}_{0.8}\text{Ag}_{0.2}\text{MnO}_3$  (LAMO) nanoparticles with mean particle sizes of 16 and 21 nm have been investigated by measuring the AC magnetic susceptibility and electron spin resonance (ESR) spectra. The obtained results from AC magnetic

✉ Ali Rostamnejadi  
ali@ph.iut.ac.ir

<sup>1</sup> Electroceram Research Center, Malek Ashtar University of Technology, Shahin Shahr, Isfahan, Iran

susceptibility show strong magnetic interaction between nanoparticles of LAMO. Electron spin resonance results indicate the magnetic phase separation in nanoparticles of LAMO at room temperature.

## 2 Experiment

Nanoparticles of LAMO have been prepared by sol-gel method [12, 19, 33]. As starting materials, stoichiometric amounts of  $\text{La}(\text{NO}_3)_3 \cdot 6\text{H}_2\text{O}$ ,  $\text{Mn}(\text{NO}_3)_2 \cdot 4\text{H}_2\text{O}$ , and  $\text{Ag}(\text{NO}_3)$  were dissolved in water and mixed with ethylene glycol and citric acid. The solution was then heated on a thermal plate under constant stirring at  $80^\circ\text{C}$  to eliminate the excess water and to obtain a viscous gel. The gel was dried at  $150^\circ\text{C}$  and then calcinated at  $500^\circ\text{C}$  for 4 h. Two packages of the obtained powder were sintered at  $600^\circ\text{C}$  (S1) and  $700^\circ\text{C}$  (S2) for 4 h to obtain nanoparticles with different particle sizes. The XRD pattern is used to check the phase formation and crystal structure of the samples, using  $\text{Cu } \alpha$  radiation source in the  $2\theta$  scan range from  $20^\circ$  to  $80^\circ$ . The average particle sizes of the samples were estimated from the X-ray peak width by using Scherrer's formula and a TEM micrograph. The AC magnetic susceptibility has been studied versus temperature in the frequency range of 40–1000 Hz and in an AC magnetic field of 800 A/m, using a Lake Shore AC susceptometer model 7000. ESR study is carried out using a Bruker X-band EMX ESR spectrometer with a microwave frequency of 9.8 GHz by sweeping the magnetic field at room temperatures. The powder sample was contained within a spin free quartz tube (inner diameter 4 mm, outer diameter 6 mm, 14 cm length) that was inserted into a  $\text{TM}_{110}$  mode cavity. The spectrometer was operated in standard absorption mode under slow passage conditions with 100 kHz field modulation.

## 3 Results and Discussion

### 3.1 Crystal Structure

X-ray diffraction is used to check the phase formation and crystal structure of the samples. The XRD pattern of the sample sintered at  $500^\circ\text{C}$ , which is not given here, shows that it is almost amorphous. By increasing the sintering temperature to  $600^\circ\text{C}$ , the perovskite structure is formed. The FULLPROF program has been used to analyze the XRD pattern of the samples [34]. The samples are found to be single phase without any noticeable trace of impurities. Figure 1 shows the XRD pattern of an S2 sample with its Rietveld analysis. The Rietveld analysis of the XRD pattern shows that the crystal structure of the samples is rhombohedral with space group  $R\bar{3}C$ , and from it, the lattice

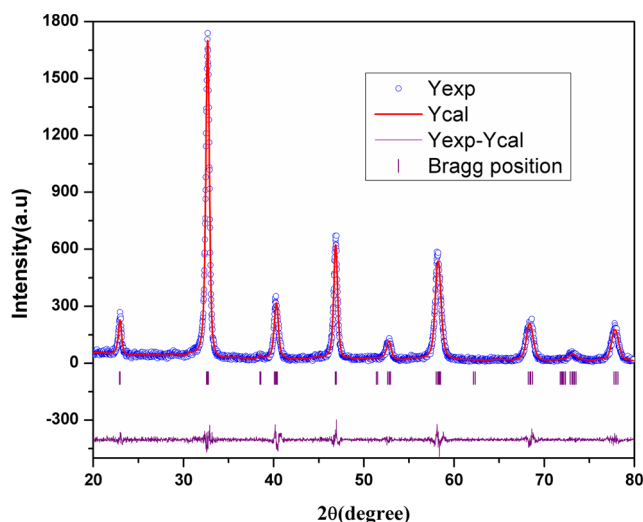


**Fig. 1** The observed and calculated (Rietveld analysis) XRD patterns of the S2 sample at room temperature

parameters  $a = 5.457$  and  $5.475 \text{ \AA}$  and  $c = 13.445$  and  $13.492 \text{ \AA}$  and the unit cell volume  $V = 346.761$  and  $350.175 \text{ \AA}^3$  are obtained for S1 and S2 samples, respectively. The average particle size of the samples can be estimated from the XRD line broadening by Scherrer's formula,

$$d = \frac{k\lambda}{\beta \cos \theta} \quad (1)$$

Here,  $\lambda = 1.5405 \text{ \AA}$  is the wavelength of  $\text{Cu } \alpha$  radiation,  $k$  is a particle shape factor and is 0.9 for spherical nanoparticles,  $\beta$  is the full width at half maximum of the XRD peak, and  $\theta$  is the diffraction angle of the peak [35]. The average particle sizes of 16 and 21 nm are obtained for S1 and S2 samples, respectively. A TEM micrograph of the S2 sample is shown

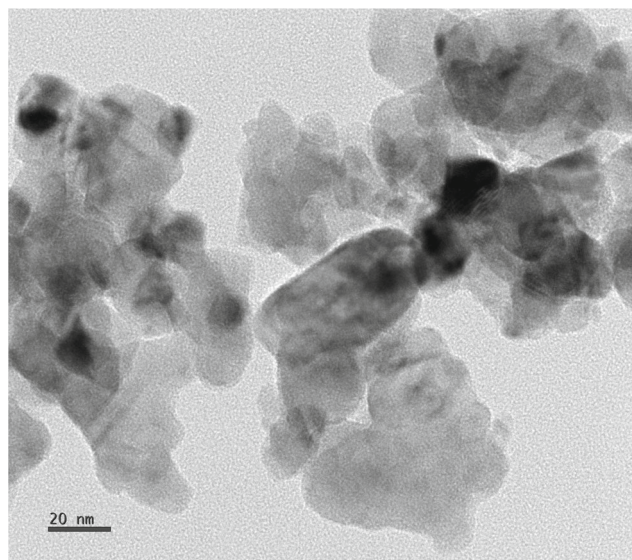


**Fig. 2** The TEM micrograph of the S2 sample

in Fig. 2. The TEM micrograph shows that the particle size distribution is almost homogenous and the mean particle size is about 22 nm, which is comparable with the average particle size calculated from the XRD line broadening.

### 3.2 AC Magnetic Susceptibility

The static and dynamic properties of magnetic nanoparticles are strongly dependent on their intrinsic and extrinsic parameters such as saturation magnetization, effective magnetic anisotropy, size and shape of the particles, temperature, and interaction between the particles and the external magnetic field [14, 16, 17, 19–23, 36–39]. Thermal energy strongly affects the magnetic properties of single domain nanoparticles and causes a superparamagnetic state in an ensemble of magnetic nanoparticles [14, 16, 17, 19–22, 36–38]. In the superparamagnetic state, the magnetization direction of the nanoparticle rapidly fluctuates between easy

axis directions. The AC magnetic susceptibility is a useful technique to study the dynamic properties of magnetic nanoparticles [19, 22, 40, 41]. Frequency dependence of the blocking temperature can be investigated by this technique. In superparamagnetic systems, the temperature dependence of the AC magnetic susceptibility has a characteristic maximum which shows the onset of the blocking process [19, 22, 40–42]. Figures 3 and 4 show the AC magnetic susceptibility of the samples versus temperature at an AC magnetic field of 800 A/m and in the frequency range of 40–1000 Hz. From Figs. 3 and 4, it can be seen that the Curie temperatures of S1 and S2 samples are about 250 and 280 K, respectively. It can be also seen that the AC magnetic susceptibilities have characteristic peaks around 225 and 245 K for the samples which may be due to the blocking/freezing process of the nanoparticle magnetization. The position of this peak is increased by increasing the applied frequency. Two well-known empirical models are used to describe

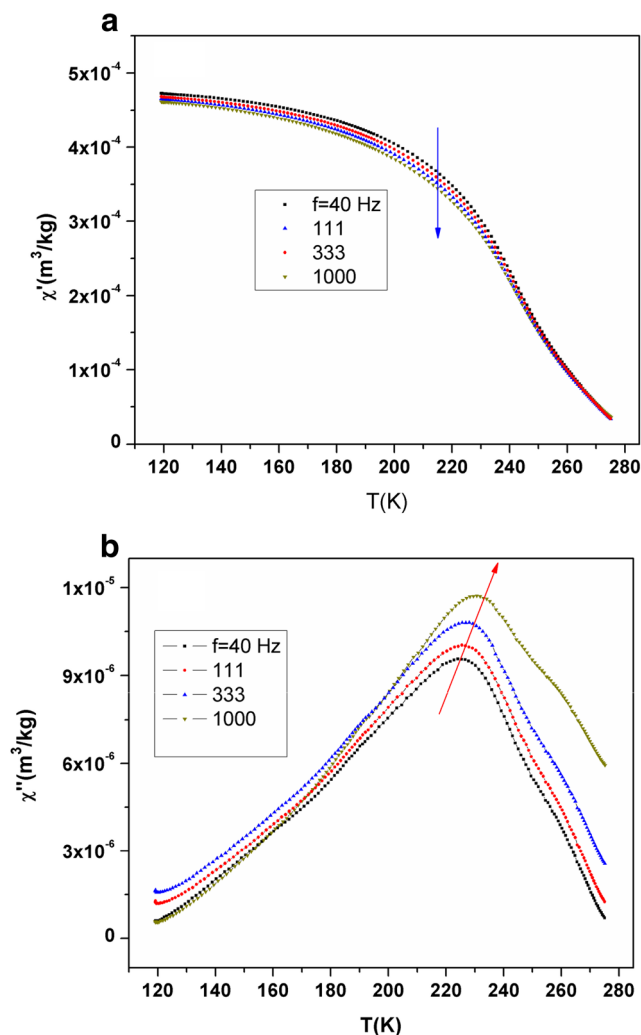


**Fig. 3** AC magnetic susceptibility of the S1 sample. **a** Real part and **b** imaginary part

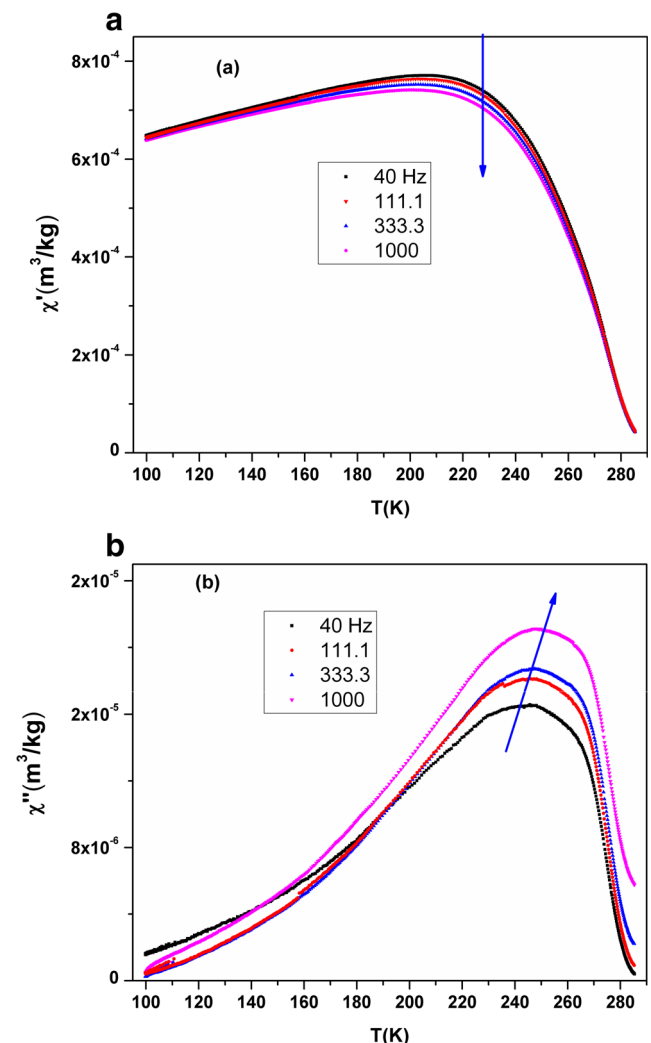


**Fig. 4** AC magnetic susceptibility of the S2 sample. **a** Real part and **b** imaginary part

the dynamic magnetic properties of magnetic nanoparticles in the superparamagnetic state. In the noninteracting superparamagnetic state, the frequency dependence of the blocking temperature can be described by the Néel-Brown model [19, 40, 41],

$$\tau = \tau_0 \exp\left(\frac{E_a}{k_B T_B}\right) \quad (2)$$

In this relation  $E_a$  is the anisotropy energy,  $T_B$  is the blocking temperature,  $\tau = 1/f$  and  $f$  is the applied frequency, and  $1/\tau_0$  is the attempt frequency. The reported values of the relaxation time  $\tau_0$  for superparamagnetic systems are in the range of  $10^{-9}$ – $10^{-13}$  s [3, 6–8]. In noninteracting single domain magnetic nanoparticles, the energy of barrier  $E_a$  can be estimated as [43]

$$E_a = k_{\text{eff}} V \sin^2 \theta \quad (3)$$

Here,  $V$  is the volume of the particle,  $k_{\text{eff}}$  is an effective magnetic anisotropy constant, and  $\theta$  is the angle between the easy axis of the particle and its magnetization. At temperatures above the blocking temperature, the thermal energy dominates the potential barrier and magnetization can follow the direction of the applied magnetic field. Below the blocking temperature, the anisotropy energy overcomes the thermal energy and magnetization of the nanoparticles is randomly blocked in their easy directions and magnetic susceptibility is reduced by decreasing the temperature [19]. As shown in Fig. 5, by fitting the experimental data from AC magnetic susceptibility with Eq. (2), unphysical values of  $\tau_0 \sim 10^{-48}$  s and  $\tau_0 \sim 10^{-80}$  s are obtained for S1 and S2 samples, respectively. Deviation from the Néel-Brown model suggests that there exists a magnetic interaction between LAMO nanoparticles. The dipolar or exchange interactions between magnetic nanoparticles increase the

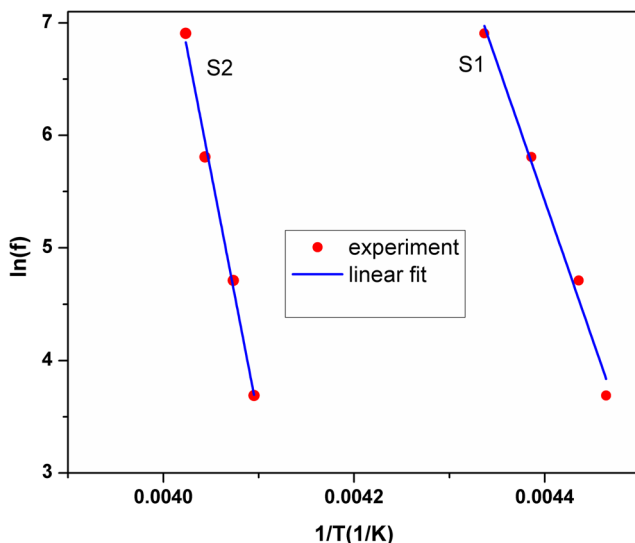


**Fig. 5**  $\ln(f)$  versus  $1/T$  for S1 and S2 samples

potential barrier, and the blocking temperature increases. In the interacting superparamagnetic state, the frequency dependence of the blocking temperature can be evaluated by the empirical Vogel-Fulcher model,

$$\tau = \tau_0 \exp\left(\frac{E_a}{k(T_B - T_0)}\right) \quad (4)$$

In this model,  $T_0$  is an effective temperature indicating interaction between nanoparticles and  $T_B$  is the blocking temperature (i.e., peak position in AC magnetic susceptibility versus temperature). In Fig. 6, the experimental data are well fitted by the Vogel-Fulcher model. From this model, the values  $T_0 = 207 \pm 3$  and  $212 \pm 5$  K,  $\tau_0 \approx 1.7 \times 10^{-7}$  and  $1 \times 10^{-13}$  s, and  $E_a/k \approx 173 \pm 10$  and  $850 \pm 10$  K are obtained for S1 and S2 samples, respectively. The agreement of experimental data with the Vogel-Fulcher law indicates the interacting superparamagnetic behavior of LAMO nanoparticles. Based on Vogel-Fulcher law, the effective magnetic anisotropy constant can be estimated from the AC magnetic susceptibility. Using the average particle size of the samples, the effective magnetic anisotropy constants of  $1.3 \times 10^4$  and  $2.8 \times 10^4$  erg/cm<sup>3</sup> are obtained for S1 and S2 samples, respectively. These values are consistent with the values reported for nanoparticles and a single crystal of LSMO ( $1.8 \times 10^4$  erg/cm<sup>3</sup>) [17, 19, 44].

The existence of a strong interaction between magnetic nanoparticles can lead to a collective superspin glass state. Two phenomenological parameters  $c_1$  and  $c_2$  are usually used to distinguish between superparamagnetic behavior and superspin glass state [2, 5, 17].

$$c_1 = \frac{\Delta T_f}{T_f \Delta(\log_{10} f)} \quad (5)$$

$$c_2 = \frac{T_f - T_0}{T_f} \quad (6)$$

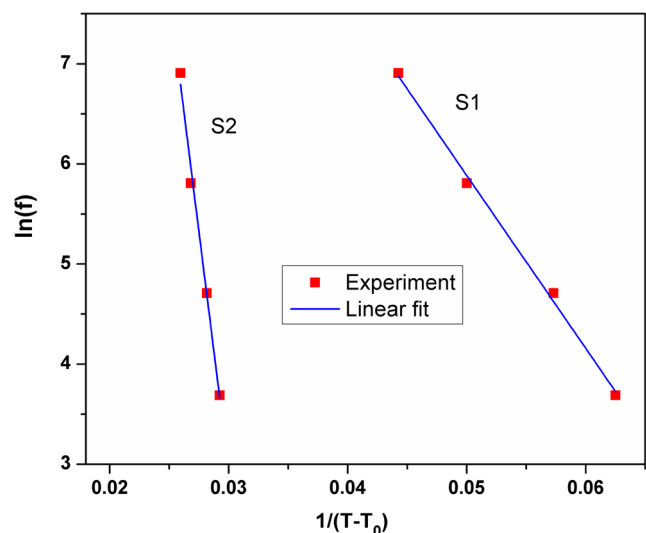


**Fig. 6**  $\ln(f)$  versus  $1/(T - T_0)$  for S1 and S2 samples

where  $T_f$  is the average blocking temperature in the range of applied frequencies,  $\Delta T_f$  is the blocking temperature difference at the  $\Delta(\log_{10} f)$  frequency interval, and  $T_0$  is a characteristic temperature which can be obtained from the Vogel-Fulcher model. The  $c_1$  parameter is independent of any model and shows the relative shift of the blocking temperature per decade of applied frequency. The  $c_2$  parameter can be used to compare the blocking/freezing temperature in various systems. There are different types of dynamic magnetic behaviors in superparamagnetic and spin glass systems that can be distinguished based on  $c_1$  and  $c_2$  values: (1) in noninteracting superparamagnetic systems, the values of  $c_1$  are in the range of 0.1–0.13 and  $c_2 = 1$  (theory); (2) for a weak interaction regime, the values of  $c_1$  and  $c_2$  are in the ranges of 0.03–0.06 and 0.3–0.6, respectively; and (3) for the medium to strong interaction regime, the values of  $c_1$  and  $c_2$  are in the ranges 0.005–0.02 and 0.07–0.3, respectively [40, 41]. The values of both  $c_1$  and  $c_2$  parameters decrease by increasing the strength of the magnetic interactions between nanoparticles. In our case, the obtained value of  $c_1$  ( $c_2$ ) is 0.02 (0.10) for the S1 sample and is 0.01 (0.14) for the S2 sample, which indicate the finite interaction between LAMO nanoparticles.

The possibility of the spin glass state in LAMO nanoparticles can be checked by the critical slowing down model. In this model, the divergence of relaxation time  $\tau$  at the transition temperature is given by

$$\tau = \tau_0(T/T_g - 1)^{-z\nu} \tag{7}$$

Here,  $T_g$  is the spin glass transition temperature,  $\tau_0$  is the relaxation time of the individual particle magnetization,  $z$  is the exponent relates relaxation time and correlation length as  $\tau \propto \xi^z$ , and  $\nu$  is the critical exponent of correlation

length,  $\xi \approx (T/T_g - 1)^{-\nu}$  and [16, 20, 22, 40]. A true equilibrium thermodynamic phase can be checked by divergence of the relaxation time or correlation length at  $T_g$ . A log-log plot of the applied frequency ( $f$ ) versus  $(T - T_g)/T_g$  is shown in Fig. 7, which shows excellent linear dependence for both samples. For  $T_g = 217 \pm 3$  K ( $220 \pm 5$  K), the relaxation time  $\tau_0 = 2 \times 10^{-9}$  s ( $1 \times 10^{-20}$  s) and critical exponent  $z\nu = 5$  (19) are obtained for S1 (S2), respectively. The estimated values of  $\tau_0$  are different from those predicted by the Vogel-Fulcher law. For spin glass systems, typical values of relaxation time  $\tau_0$  are in the range of  $10^{-9}$ – $10^{-12}$  s and the critical exponent  $z\nu$  are in the range 7–12 [17, 21, 22]. Therefore, the obtained values of  $z\nu$  and  $\tau_0$  of the samples are not consistent with those expected for the spin glass systems. These results suggest that in LAMO nanoparticles,

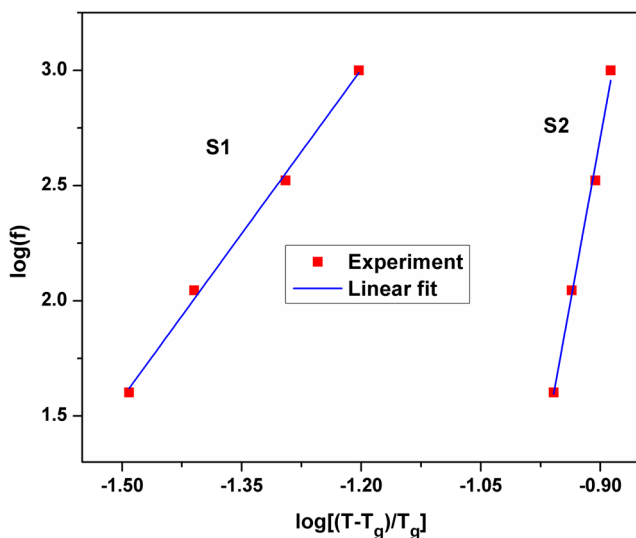


**Fig. 7** A log-log plot of frequency versus reduced temperature for S1 and S2 samples

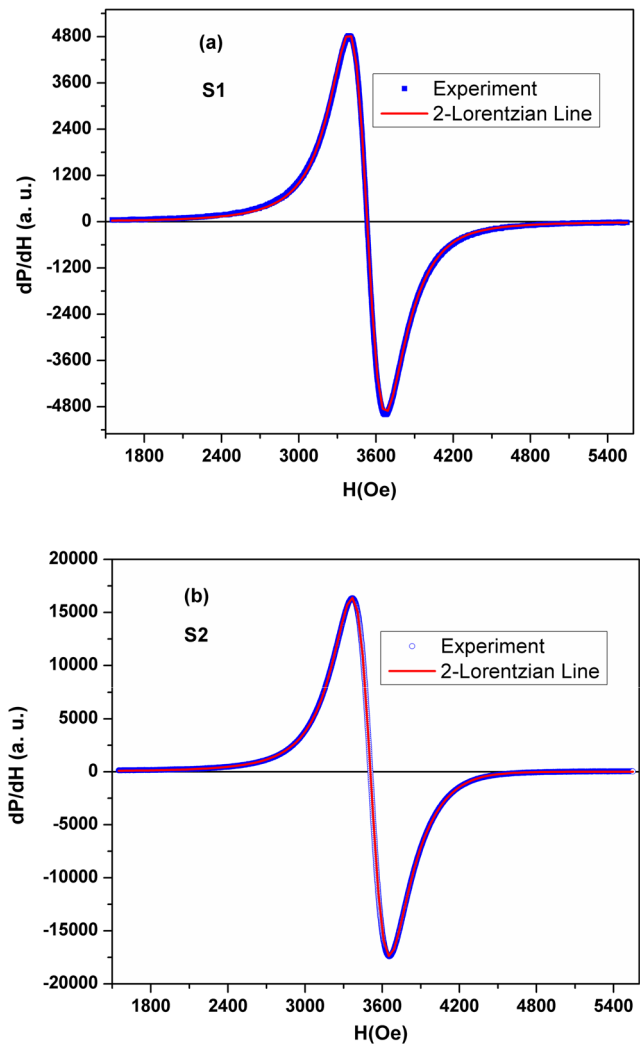


**Fig. 8** Electron spin resonance spectra of LAMO samples at room temperature. **a** The ESR absorption spectra of the S1 sample and **b** the ESR absorption spectra of the S2 sample. *Continuous lines* showing double Lorentzian line fitting



blocking of the interacting particles occurs rather than the spin glass state.

### 3.3 Electron Spin Resonance

Microwave properties are investigated by measuring the electron spin resonance of the samples at room temperature. Electron spin resonance is a highly sensitive dynamical technique which can give valuable information about the phase separation and phase transition in magnetic materials [45, 46]. The ESR signals of the samples have been measured at room temperature and are shown in Fig. 8. It can be seen from Fig. 8 that the ESR signals of the samples are almost symmetric and well fitted to a double Lorentzian line shape as [45]

$$\frac{dP}{dH} = y_0 + \frac{d}{dH} \left[ \frac{2A_1}{\pi} \left( \frac{w_1}{4(H - H_1)^2 + w_1^2} \right) + \frac{2A_2}{\pi} \left( \frac{w_2}{4(H - H_2)^2 + w_2^2} \right) \right] \quad (8)$$

In this relation,  $H_1$  and  $H_2$  are the center fields,  $w_1$  and  $w_2$  are the full widths at half maximum, and  $A_1$  and  $A_2$  are proportional to the area under the curves. The obtained values for both samples are given in Table 1. The origin of the two ESR signals comes from the possible magnetic phase separation in LAMO nanoparticles which in the paramagnetic state there is a ferromagnetic phase [47–52]. The ESR signal with lower resonance field  $H_1$  and line with  $w_1$  is attributed to paramagnetic spin resonance of  $Mn^{3+}$  and  $Mn^{4+}$  ions, while the second signal with higher resonance field  $H_2$  and line with  $w_2$  is due to the presence of ferromagnetic clusters in the paramagnetic state. The ferromagnetic state in manganite is due to the double exchange interaction between  $Mn^{3+}$  and  $Mn^{4+}$  ions [1]. It can be seen from Table 1 that by increasing the particle size, the intensity of the ferromagnetic signal is increased. The  $g$ -values of the

samples are obtained from the resonance condition  $\nu = \mu_B H_r$  [53]. For the signal with lower resonance field  $H_1$ , the  $g$ -values are 1.98 and 1.99 for S1 and S2 samples, respectively, which are consistent with the paramagnetic phase. For the signal with higher resonance field  $H_2$ , the  $g$ -values are 1.75 and 1.77 for S1 and S2 samples, respectively, which are due to ferromagnetic clusters at room temperature.

### 4 Conclusions

In this research, single phase magnetic nanoparticles of  $La_{0.8}Ag_{0.2}MnO_3$  with mean particle sizes of 16 and 21 nm have been prepared by sol-gel method. The AC magnetic susceptibilities of the samples show a characteristic peak which is frequency dependent and suggests the blocking/freezing processes in nanoparticles of  $La_{0.8}Ag_{0.2}MnO_3$ . The dynamic behaviors of the samples are described by two empirical  $c_1$  and  $c_2$  parameters, Neel-Brown, Vogel-Fulcher, and critical slowing down models. The obtained values of  $c_1$  and  $c_2$  show the interacting superparamagnetic behavior in LAMO nanoparticles. The relaxation times obtained from the Neel-Brown model have small unphysical values which indicate the presence of magnetic interaction between LAMO nanoparticles. Frequency dependence of the blocking temperature is well described by the Vogel-Fulcher model which confirms the existence of a strong interaction between nanoparticles of LAMO. The experimental data are also fitted by the critical slowing down model which gives unacceptable values for relaxation time and critical exponent. Because of the common behaviors, it is difficult to distinguish between superparamagnetic and real spin glass systems by AC magnetic susceptibility and other techniques like aging and magnetic memory effects can be used. Electron spin resonance signals of the samples at room temperature are fitted by double Lorentzian line shapes which indicate the presence of ferromagnetic clusters in the paramagnetic state.

**Table 1** Electron spin resonance parameters of the samples obtained from double Lorentzian line shapes and the resonance condition

Parameters	S1	S2
$y_0$ (a. u.)	0.8	12
$A_1$ (a. u.)	$1.4 \times 10^9$	$5.2 \times 10^9$
$A_2$ (a. u.)	$5.8 \times 10^7$	$1.1 \times 10^9$
$A_1/A_2$	24.1	4.7
$w_1$ (Oe)	492.1	503.3
$w_2$ (Oe)	988.5	1257.6
$H_1$ (Oe)	3532.1	3511.1
$g_1$	1.98	1.99
$H_2$ (Oe)	4007.1	3965.1
$g_2$	1.75	1.77

**Acknowledgments** The author is thankful to Prof. Hadi Salami for providing experimental facilities and Dr. Karl Ackland for electron spin resonance measurement.

### References

1. Coey, J.M.D., Viret, M., Von Molnar, S.: *Adv. Phys.* **58**, 571 (2009)
2. Dagotto, E.: *Nanoscale Phase Separation and Colossal Magnetoresistance: the Physics of Manganites and Related Compounds*. Springer Verlag (2003)
3. Dagotto, E.: *New J. Phys.* **7**, 67 (2005)
4. Mercone, S., Perroni, C.A., Cataudella, V., Adamo, C., Angeloni, M., Aruta, C., De Filippis, G., Miletto, F., Oropallo, A., Perna, P.,

- Petrov, A.Y., Scotti di Uccio, U., Maritato, L.: *Phys. Rev. B* **71**(6), 064415 (2005)
5. Lopez-Quintela, M., Hueso, L., Rivas, J., Rivadulla, F.: *Nanotech.* **14**, 212 (2003)
  6. Haghiri-Gosnet, A., Renard, J.: *J. phys. D : Appl. Phys.* **36**, R127 (2003)
  7. Bingham, N., Phan, M., Srikanth, H., Torija, M., Leighton, C.: *J. App. Phys.* **106**(2), 023909 (2009)
  8. Zhu, T., Shen, B., Sun, J., Zhao, H., Zhan, W.: *Appl. Phys. Lett.* **78**(24), 3863 (2001)
  9. Roy, S., Dubenko, I., Edoth, D.D., Ali, N.: *J. App. Phys* **96**, 1202 (2004)
  10. Roy, B., Poddar, A., Das, S.: *J. Appl. Phys.* **100**, 104318 (2006)
  11. Roy, B., Das, S.: *J. App. Phys.* **104**(10), 103915 (2008)
  12. Rostamnejadi, A., Venkatesan, M., Alaria, J., Boese, M., Kameli, P., Salamati, H., Coey, J.: *J. Appl. Phys.* **110**, 043905 (2011)
  13. Nath, T., Dutta, P., Dey, P.: *J. Appl. Phys.* **103**(7), 07F725 (2008)
  14. Thakur, M., Patra, M., Majumdar, S., Giri, S.: *J. Appl. Phys.* **105**(7), 073905 (2009)
  15. Fiorani, D., Dormann, J., Cherkaoui, R., Tronc, E., Lucari, F., D'orazio, F., Spinu, L., Nogues, M., Garcia, A., Testa, A.: *J. Magn. Magn. Mater* **196**, 143 (1999)
  16. Dormann, J., Fiorani, D., Cherkaoui, R., Tronc, E., Lucari, F., D'orazio, F., Spinu, L., Nogues, M., Kachkachi, H., Jolivet, J.: *J. Magn. Magn. Mater* **203**(1–3), 23 (1999)
  17. Rostamnejadi, A., Salamati, H., Kameli, P.: *J. Supercon. Nov. Magn.* **25**(4), 1123 (2012)
  18. Markovic, D., Kusigerski, V., Tadic, M., Blanusa, J., Antisari, M.V., Spasojevic, V.: *Scripta Mater* **59**(1), 35 (2008)
  19. Rostamnejadi, A., Salamati, H., Kameli, P., Ahmadvand, H.: *J. Magn. Magn. Mater* **321**(19), 3126 (2009)
  20. Dormann, J., Bessais, L., Fiorani, D.: *J. Phys. C: Solid State Phys* **21**, 2015 (1988)
  21. Bedanta, S., Kleemann, W.: *J. Phys. D: Appl. Phys.* **42**, 013001 (2009)
  22. Jönsson, P.E.: *Adv. Chem. Phys.*, 191 (2004)
  23. Li, R.W., Xiong, H., Sun, J.R., Li, Q.A., Wang, Z.H., Zhang, J., Shen, B.G.: *J Phys.: Cond. Matter* **13**, 141 (2001)
  24. Atsarkin, V., Generalov, A., Demidov, V., Mefed, A., Markelova, M.: *J. Comm. Tech. Elec* **55**(6), 657 (2010)
  25. Gamzatov, A., Batdalov, A.: *Phys. Solid State* **54**(1), 70 (2012)
  26. Gamzatov, A., Batdalov, A., Kamilov, I.: *Physica B: Cond. Matter* **406**(11), 2231 (2011)
  27. Huang, S., Deng, L., Zhou, K., Hu, Z., Sun, S., Ma, Y., Xiao, P.: *J. Magn. Magn. Mater* (2012)
  28. Ye, S., Song, W., Dai, J., Wang, K., Wang, S., Zhang, C., Du, J., Sun, Y., Fang, J.: *J. Magn. Magn. Mater* **248**(1), 26 (2002)
  29. Xu, Q., Wang, R., Zhang, Z.: *phys. Rev. B* **71**(9), 092401 (2005)
  30. Teplykh, A., Bogdanov, S., Valiev, É., Pirogov, A., Dorofeev, Y.A., Ostroushko, A., Udilov, A., Kazantsev, V., Kar'kin, A.: *Phys. Sol. State* **45**(12), 2328 (2003)
  31. Shlyakhtin, O., Leontiev, V., Oh, Y.-J., Kuznetsov, A.: *Smart Mate. Stru* **16**(5), N35 (2007)
  32. Gamzatov, A., Batdalov, A., Kamilov, I., Kaul, A., Babushkina, N.: *Appl. Phys. Lett.* **102**(3), 032404 (2013)
  33. Rostamnejadi, A., Venkatesan, M., Kameli, P., Salamati, H., Coey, J.: *J. Magn. Magn. Mater* **323**(16), 2214 (2011)
  34. Rodríguez-Carvajal, J.: *Physica B: Cond. Matter* **192**(1–2), 55 (1993)
  35. Sharma, S., Kumar, R., Kumar, S., Siva Kumar, V., Knobel, M., Reddy, V., Banerjee, A., Singh, M.: *Sol. Stat. Comm* **141**(4), 203 (2007)
  36. Markovich, V., Jung, G., Wisniewski, A., Puzniak, R., Fita, I., Yuzhelevski, Y., Mogilyansky, D., Titelman, L., Gorodetsky, G.: *J. Supercond. Nov.Magn.* **1**(2), 861 (2011)
  37. Kumar, N., Kumar, A., Jha, R., Dogra, A., Pasricha, R., Kotnala, R., Kishan, H., Awana, V.P.S.: *J. Supercond. Nov. Magn* **23**(4), 423 (2010)
  38. Suzuki, M., Fullem, S.I., Suzuki, I.S., Wang, L., Zhong, C.J.: *Phys. Rev. B* **79**(2), 024418 (2009)
  39. Karaagac, O., Kockar, H., Tanrisever, T.: *J. Supercond. Nov. Magn.*, 1 (2011)
  40. Dormann, J., Fiorani, D., Tronc, E.: *Adv. Chem. Phys* **98**, 283 (1997)
  41. Dormann, J., Fiorani, D., Tronc, E.: *J. Magn. Magn. Mater* **202**(1), 251 (1999)
  42. Parker, D., Dupuis, V., Ladiou, F., Bouchaud, J.P., Dubois, E., Perzynski, R., Vincent, E.: *Phys. Rev. B* **77**(10), 104428 (2008)
  43. Goya, G., Berquo, T., Fonseca, F., Morales, M.: *J. Appl. Phys.* **94**, 3520 (2003)
  44. Suzuki, Y., Hwang, H., Cheong, S., Siegrist, T., Van Dover, R., Asamitsu, A., Tokura, Y.: *J. Appl. Phys.* **83**, 7064 (1998)
  45. Rao, S.S., Padmanabhan, B., Elizabeth, S., Bhat, H.L., Bhat, a.S.V.: *J. Phys. D: Appl. Phys.* 41 (2008)
  46. Likodimos, V., Pissas, a.M.: *J. Phys.: Condens. Matter* (2005)
  47. Deisenhofer, J., Braak, D., Krug von Nidda, H.A., Hemberger, J., Eremina, R.M., Ivanshin, V.A., Balbashov, A.M., Jug, G., Loidl, A., Kimura, T., Tokura, Y.: *Phys. Rev. Lett.* **95**(25), 257202 (2005)
  48. Jiang, W., Zhou, X., Williams, G., Mukovskii, Y., Glazyrin, K.: *Phys. Rev. B* **77**(6), 064424 (2008)
  49. Lu, W., Luo, X., Hao, C., Song, W., Sun, Y.: *J. Appl. Phys.* **104**(11), 113908 (2008)
  50. Rama, N., Ramachandra Rao, M.S., Sankaranarayanan, V., Majewski, P., Gepreags, S., Opel, M., Gross, R.: *Phys. Rev. B* **70**(22), 224424 (2004)
  51. Salamon, M.B., Lin, P., Chun, S.H.: *Phys. Rev. Lett.* **88**(19), 197203 (2002)
  52. Tong, P., Kim, B., Kwon, D., Qian, T., Lee, S.-I., Cheong, S.W., Kim, B.G.: *Phys. Rev. B* **77**(18), 184432 (2008)
  53. Coey, J.M.D.: *Magnetism and Magnetic Materials*. Cambridge University Press (2010)